31st Annual International Conference of the IEEE EMBS
Minneapolis, Minnesota, USA, September 2-6, 2009

Deblurring Molecular Images Using Desorption Electrospray Ionization Mass Spectrometry

R. Mitchell Parry, *Member, IEEE*, Asiri S. Galhena, Facundo M. Fernandez, and May D. Wang, *Member, IEEE*

***Abstract*—Traditional imaging techniques for studying the spatial distribution of biological molecules such as proteins, metabolites, and lipids, require the *a priori* selection of a handful of target molecules. Imaging mass spectrometry provides a means to analyze thousands of molecules at a time within a tissue sample, adding spatial detail to proteomic, metabolomic, and lipidomic studies. Compared to traditional microscopic images, mass spectrometric images have reduced spatial resolution and require a destructive acquisition process. In order to increase spatial detail, we propose a constrained acquisition path and signal degradation model enabling the use of a general image deblurring algorithm. Our analysis shows the potential of this approach and supports prior observations that the effect of the sprayer focuses on a central region much smaller than the extent of the spray.**

I. Introduction

IMAGING mass spectrometry (MS) provides a high-throughput method for assaying the biomolecular content (e.g., proteins, peptides, metabolites, and lipids) within a two-dimensional biological sample [1, 2]. Unlike molecular imaging techniques such as immunohistochemistry (IHC) or quantum dot (QD) staining that target predefined molecules, imaging-MS profiles thousands of potentially interesting species simultaneously. This increase in molecular detail comes at the cost of spatial resolution. IHC and QD staining directly affect the optical properties of molecules of interest revealed in microscopic images with resolution limited only by the resolution of light microscopy and the size of the reporter molecule. For example, single nanoscale QDs can be identified using fluorescence microscopy. In contrast, imaging-MS must forcibly desorb or extract molecules for detection within a mass spectrometer. For desorption electrospray ionization, this extraction process affects regions of sample currently much larger than a single cell. Therefore, current research attempts to fine-tune instrumentation and sample preparation to increase spatial resolution [3]. We propose a deconvolution technique that takes into account signal degradation and show its suitability for improving the spatial resolution of imaging-MS data after collection. We focus on imaging desorption electrospray ionization mass spectrometry (DESI-MS) for imaging [4] and discuss extensions to other imaging-MS technologies.

Manuscript received April 23, 2009. This work was supported in part by grants from Microsoft Research, National Institutes of Health (Bioengineering Research Partnership R01CA108468, P20GM072069, Center for Cancer Nanotechnology Excellence U54CA119338), Georgia Cancer Coalition (Distinguished Cancer Scholar Award to M. Wang), and funding from Georgia Tech for the Center for Bio-Imaging Mass Spectrometry.

R. M. Parry is with the Department of Biomedical Engineering, Georgia Institute of Technology and Emory University, Atlanta, GA 30332 USA. (e-mail: parry@bme.gatech.edu).

A. S. Galhena is with the School of Chemistry and Biology, Georgia Institute of Technology, Atlanta, GA 30332 USA.

F. M. Fernandez is with the School of Chemistry, Georgia Institute of Technology, Atlanta, GA 30332 USA. (co-corresponding author, phone: 404-385-4432; fax: 404-894-7452; e-mail: facundo.fernandez@chemistry.gatech.edu).

M. D. Wang is with the Department of Biomedical Engineering, Georgia Institute of Technology and Emory University, Atlanta, GA 30332 USA. (co-corresponding author, phone: 404-385-2954; fax: 404-385-4243; e-mail: maywang@ bme.gatech.edu).

II. Imaging DESI-MS

In DESI-MS experiments, the charged droplets produced by an electrospray are pneumatically directed at high velocities toward the surface [5]. There are two possible outcomes that may result from droplets impacting onto a surface: settling into a liquid film on the surface or splashing away from the surface [6]. Simulations of the DESI process indicate that the solid-phase analytes on the sample surface first dissolve into the deposited liquid film and then exit the surface via splashing [7]. Thus, detecting analytes with DESI-MS necessarily degrades the sample so that subsequent scans of the same spray impacted region recover fewer and fewer analytes until depleted.

In order to produce images, the instrumentation, sprayer, and capillary remain fixed while a two-dimensional stage moves the mounted sample in a predefined route. A two-dimensional raster pattern maximizes acquisition speed by minimizing the total distance that the stage moves (i.e., the stage moves left-to-right, descends to the next raster line, and then returns right-to-left). To avoid directional effects on the overall collection or transmission of analytes that enter the mass spectrometer, a "comb" pattern can alternatively be employed (i.e., after moving left-to-right, the stage moves back right-to-left on the same path before descending to the next raster line). Because we observe a difference in overall abundance between the two directions, we ignore data collected on the return path in interpolating the MS chemical image.

III. Data Collection

Typically, in an imaging-MS experiment the gap between adjacent raster lines roughly equals the radius of the sprayed

region. However, in an attempt to increase the resolution of DESI-MS images, the distance between scans can be made much smaller. For example, in our test case we use a sprayer that projects onto an approximately 200 μm radius. We use a gap spacing of 50 μm and record scans approximately every 50 μm. Therefore, adjacent scans contain information regarding highly overlapping sample regions.

We control the sample stage using LabVIEW automation software (National Instruments Corporation, Austin, TX) and), and the MS instrument using Xcalibur V2.0 (Thermo Finnigan)). The MS instrument reports sequential mass spectra profiles and a time-stamp for each scan. The stage control software records the time when it changes direction. Using this information, we approximate a constant stage speed for each leg of the path. The position of each scan is linearly interpolated between the known time-position pairs from the stage control software and the scan's time-stamp from the MS instrument. Because the clock on the MS instrument is not synchronized with the clock on the stage control software, we select a small time-delay to compensate. Finally, to produce a discrete pixel image, we linearly interpolate molecular abundances for linearly spaced bins on each scan-line. We choose the number of pixels per image-row of the image as the average number of scans per line, and the number of pixels per image-column as the number of unique scan-lines. This results in roughly 50 μm × 50 μm pixels.

IV. Image Deblurring and Deconvolution

The inherent properties of an image acquisition method often introduce systematic blurriness. A point spread function (PSF) defines this blurriness as the spatial distribution of a theoretical point source [8]. Ideally, the image would reveal a single infinitesimal signal; however, the PSF broadens the spatial extent of this signal. For digital images, the PSF can extend to neighboring pixels causing blurring. This process is represented by a two-dimensional convolution of the PSF and the true deblurred image:

$$Y[m,n] = \sum_{u=-n_u}^{n_u} \sum_{v=-n_v}^{n_v} X[m+u,n+v]P[u,v] + N[m,n], \quad (1)$$

where X is the $M \times N$ original image, P is the $(2n_u+1)\times(2n_v+1)$ point spread function, Y is the $M \times N$ blurred image, N is additive noise, and indices outside the range of X are ignored. All elements of X, Y, and P are non-negative.

When the PSF is known in advance (e.g. from theoretical properties of the image acquisition system), X can be estimated using image restoration algorithms [9]. Image identification is the problem of estimating the degradation system including the PSF and statistical properties of Y and N [9]. Estimating X and P given only Y comprises concurrent image identification and restoration.. When modeled by (1), this corresponds to the *blind* image deconvolution problem for which a variety of algorithms exist [10, 11]. The key difference for applying these algorithms to mass spectrometry images is that the underlying "deblurred" image changes during the acquisition process. That is, each scan extracts analytes that can never be extracted again. Only a fraction of the original analytes remains for a subsequent scan on an overlapping region.

V. Incorporating Sample Degradation into the PSF

We model the DESI-MS image acquisition as a discrete process that concurrently degrades and detects analytes in a two-dimensional sample. The degradation kernel, D, represents the fraction of analytes remaining for spatial positions within a region approximating the electrospray extent centered at the origin:

$$D = \begin{bmatrix} D[-n_u,-n_v] & \cdots & D[-n_u,n_v] \\ \vdots & \ddots & \vdots \\ D[n_u,-n_v] & \cdots & D[n_u,n_v] \end{bmatrix}. \quad (2)$$

The detection kernel, $K = 1 - D$, represents the fraction of analytes extracted from the sample and entering the MS. In this case, X is a function of time. At each time-step, with the sprayer centered at $[m,n]$, we update the underlying sample as follows:

$$X^{(t+1)}[m+u,n+v] = X^{(t)}[m+u,n+v]D[u,v]. \quad (3)$$

The MS detects the extracted analytes:

$$Y[m,n] = \sum_{u=-n_u}^{n_u} \sum_{v=-n_v}^{n_v} X^{(t)}[m+u,n+v]K[u,v] + N[m,n]. \quad (4)$$

Whereas the detection kernel has a natural interpretation as a non-normalized PSF, the effect of the degradation kernel on (1) depends on the time-dependent path of the sprayer. By rasterizing the two-dimensional sample one row at a time, we model the net effect one pass of the sprayer as the product of each row of the degradation kernel:

$$d[u] = \prod_{v=-n_v}^{n_v} D[u,v]. \quad (5)$$

Considering only the left-to-right portion of the "comb" path, we represent the current total degradation centered at the

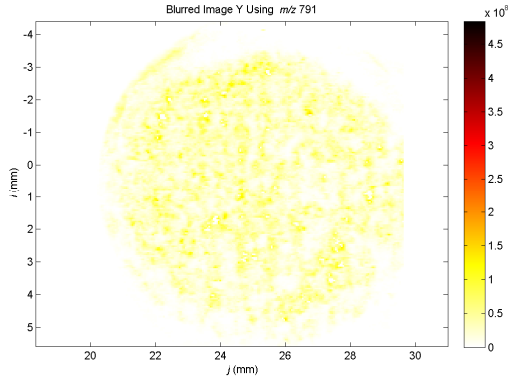

Fig. 1. Original (blurred) DESI-MS image of an artesunate antimalarial drug tablet using *m/z* 791.

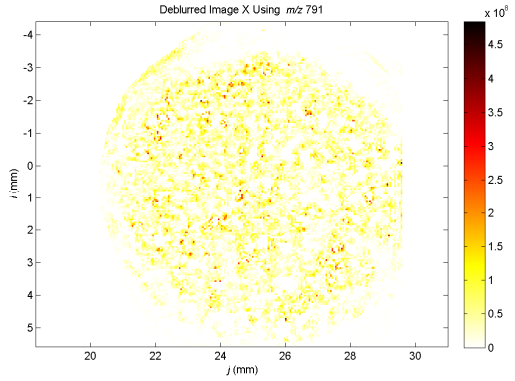

Fig. 2. Deblurred DESI-MS image using *m/z* 791. The peaks and valleys are sharper.

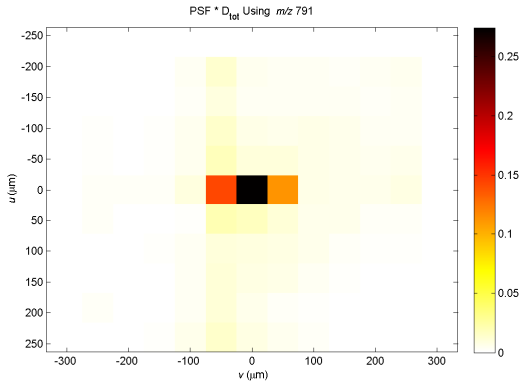

Fig. 3. Combined degradation/detection kernel P = PSF * D_{tot} for *m/z* 791.

sprayer position as:

$$D_{\text{total}}[u,v] = \left(\prod_{i=u+1}^{n_u} d[i]^2 \right) \left(\prod_{j=v+1}^{n_v} D[u,j] \right), \quad (6)$$

where the contribution from each row is squared to account for the right-to-left backtracking in the comb pattern. The degraded signal when the sprayer reaches the position $X[m,n]$ at this time point is simply the following:

$$X^{(t+1)}[m+u,n+v] = X[m+u,n+v] D_{\text{total}}[u,v]. \quad (7)$$

For this restricted path scenario, notice that the current (sprayer centered) region of the degraded sample is *not* a function of time and the degradation does *not* depend on location. Therefore, we can interpret P in (1) as the product of a detection kernel K and the total degradation:

$$P[u,v] = K[u,v] D_{\text{total}}[u,v]. \quad (8)$$

By reducing the problem of DESI-MS image deblurring to the classical problem of blind deconvolution, we may apply existing algorithms to estimate the deblurred image X and kernel P given only the blurred image, Y.

VI. Results

We apply a blind image deconvolution algorithm (`deconvblind`) provided in the MATLAB® Image Processing Toolbox™ (R2008b, The Mathworks, Inc., Natick, MA) to digital images collected using the DESI-MS setup described previously. The algorithm converges in less than 5 seconds for each of the following 200 × 209 pixel images on a 3.6 GHz machine. First, we apply the algorithm to the most common ion in an artesunate antimalarial drug tablet. Fig. 1 shows the original interpolated DESI-MS image for *m/z* 791 ([2 artesunic acid+Na]$^+$). After running the deconvolution algorithm until convergence using the "resuming" interface, Fig. 2 shows the deblurred version that contains sharper peaks and valleys. Fig. 3 shows the estimated kernel P that combines the PSF and total degradation. Generally, more analytes appear to originate toward the bottom and toward the right side of the kernel, consistent with the expected degradation model in (6). Notice, for example, the sharp decline in signal at v=-100 micrometers. The vast majority of signal comes from the row of three central pixels. This supports the observation that the effect of the sprayer focuses on a central region much smaller than the extent of the spray [3].

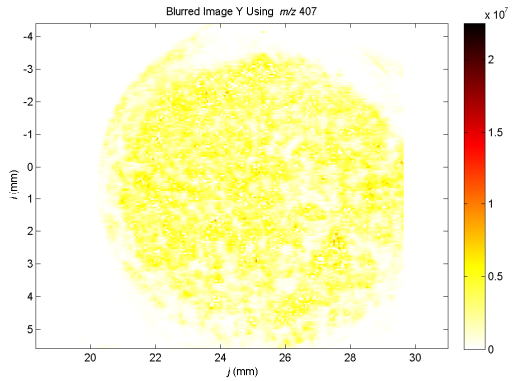

Fig. 4. Original (blurred) DESI-MS image of an artesunate antimalarial drug tablet for m/z 407.

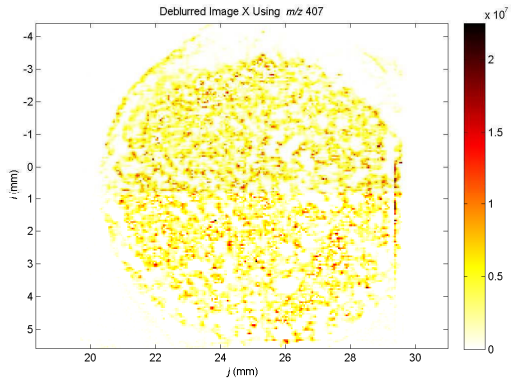

Fig. 5. Deblurred DESI-MS image for m/z 407.

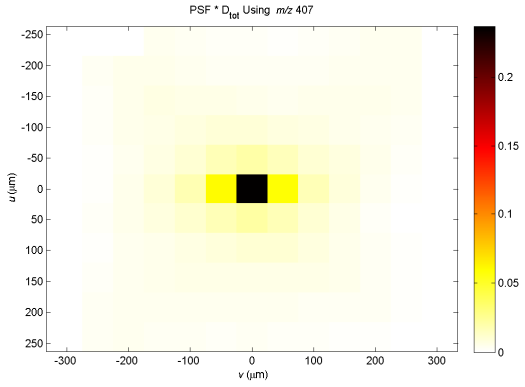

Fig. 6. Combined degradation/detection kernel P = PSF * D_{tot} for m/z 407.

We consider the possibility that the DESI extracts different analytes at different rates. This would result in a different P for each analyte. The MS instrument distinguishes between analytes based on m/z. For the same sample treated above, we examine only m/z 407 ([artesunic acid+Na]$^+$) and repeat the deblurring procedure. Fig. 4 shows the original m/z 407 image. Fig. 5 shows the estimated deblurred image containing sharper peaks. Interestingly, the kernel in Fig. 6 appears smoother and more symmetric than Fig. 3, suggesting that degradation plays a smaller role for this analyte.

VII. Conclusion

We consider the problem of molecular image deblurring for a destructive DESI-MS imaging technique. We show that for a constrained rasterization path, the deblurring problem reduces to blind image deconvolution of the blurred image into a deblurred image and the product of a degradation and detection kernel. We apply a standard algorithm, and present results that support prior observations that the effective spray region is much smaller than the spray extent (in our case a width of ~150 μm compared to ~400 μm). Future work includes tailoring the blind deconvolution algorithm to leverage the known structure of the combined degradation/detection kernel, extending it to other destructive imaging techniques such as MALDI-MS imaging, and designing controlled experiments to evaluate the accuracy of this approach.

References

[1] L. A. McDonnell and R. M. A. Heeren, "Imaging mass spectrometry," *Mass Spectrometry Reviews,* vol. 26, pp. 606-643, Jul-Aug 2007.

[2] M. L. Pacholski and N. Winograd, "Imaging with mass spectrometry," *Chemical Reviews,* vol. 99, pp. 2977-+, Oct 1999.

[3] V. Kertesz and G. J. Van Berkel, "Improved imaging resolution in desorption electrospray ionization mass spectrometry," *Rapid Communications in Mass Spectrometry,* vol. 22, pp. 2639-2644, 2008.

[4] Z. Takáts, J. M. Wiseman, B. Gologan, and R. G. Cooks, "Mass spectrometry sampling under ambient conditions with desorption electrospray ionization," *Science,* vol. 306, pp. 471-473, 2004.

[5] I. V. Roisman and C. Tropea, "Fluctuating flow in a liquid layer and secondary spray created by an impacting spray," *International Journal of Multiphase Flow,* vol. 31, pp. 179-200, Feb 2005.

[6] L. Nyadong, E. G. Hohenstein, K. Johnson, C. D. Sherrill, M. D. Green, and F. M. Fernández, "Desorption electrospray ionization reactions between host crown ethers and the influenza neuraminidase inhibitor oseltamivir for the rapid screening of Tamiflu®," *The Analyst,* vol. 133, pp. 1513-1522, 2008.

[7] A. B. Costa and R. Graham Cooks, "Simulated splashes: Elucidating the mechanism of desorption electrospray ionization mass spectrometry," *Chemical Physics Letters,* vol. 464, pp. 1-8, 2008.

[8] S. Sabri, F. Richelme, A. Pierres, A. M. Benoliel, and P. Bongrand, "Interest of image processing in cell biology and immunology," *Journal of Immunological Methods,* vol. 208, pp. 1-27, Oct 1997.

[9] R. L. Lagendijk and J. Biemond, *Iterative identification and restoration of images*. Boston: Kluwer Academic Publishers, 1991.

[10] D. Kundur and D. Hatzinakos, "Blind image deconvolution revisited," *IEEE signal processing magazine,* vol. 13, pp. 61-63, 1996.

[11] D. Kundur and D. Hatzinakos, "Blind image deconvolution," *Signal Processing Magazine, IEEE,* vol. 13, pp. 43-64, 1996.